Available online at www.sciencedirect.com

ScienceDirect

journal homepage: http://www.elsevier.com/locate/acme

Original Research Article

A new hybrid energy dissipation system with viscoelastic and flexural yielding strips dampers for multi-level vibration control

Omid Ranaei [a,*], *Ali Akbar Aghakouchak* [b,*]

[a] *Department of Smart Structures Engineering, Tarbiat Modares University, Tehran, Iran*
[b] *Department of Civil and Environmental Engineering, Tarbiat Modares University, Tehran, Iran*

ARTICLE INFO

Article history:
Received 23 June 2018
Received in revised form
1 November 2018
Accepted 14 December 2018
Available online 25 January 2019

Keywords:
Elastomeric layers
Flexural yielding strips
Hybrid damper
Energy dissipation
Analytical simulation

ABSTRACT

In this study, a new hybrid damper (HD) is introduced that consists of elastomeric layers, which act as a viscoelastic damper (VED), and metallic dampers (MDs). Metallic part is composed of flexural yielding strips. This HD not only removes the limitations of each of these two types of dampers, but also facilitates its application for multi-level vibration control. Based on operational mechanism and design objectives of the proposed HD, three specimens have been manufactured and tested under quasi-static cyclic loading to evaluate the functional objectives. Two types of elastomers and two types of metallic dampers are used in these specimens. Experimental results show stable hysteretic behavior and high energy dissipation capacity. Also, the multi-phase behavior of the proposed HD confirms the proper function that is intended. However, the HD that is made of natural rubber (NR) and comb-teeth damper (CTD) can tolerate more cycles and possesses more ductility in comparison with the HD made of butyl rubber (IIR) and steel slit damper (SSD). A finite element model (FEM) is also used to simulate the behavior of the proposed HD. A good correlation between numerical outputs, analytical equations and experimental results indicates the accuracy of the proposed FEM.

1. Introduction

Passive energy dissipation (PED) systems have been widely used in recent years to serve as structural control systems against natural hazards in order to protect structural components from damage, control the dynamic response of structures and increase the seismic resilience of structures. PED systems are classified into two categories [1–3]: (a) seismic isolator (e.g. elastomeric bearings and lead rubber bearings) [4], (b) energy dissipation devices that are subdivided into [5] displacement-dependent devices (e.g. yielding metallic damp-

* *Corresponding author.*
E-mail addresses: omid.ranaei@modares.ac.ir (O. Ranaei), a_agha@modares.ac.ir (A.A. Aghakouchak).
https://doi.org/10.1016/j.acme.2018.12.005
1644-9665/

er [6,7], friction damper [8] and buckling restrained brace [9,10]), velocity-dependent devices (e.g. viscoelastic damper [11–13] and viscous damper [14]), motion-dependent devices (e.g. tuned mass damper and tuned liquid damper [15–17]) and re-centering systems (e.g. rocking systems, post-tensioned systems, self-centering braces, etc. [18]). Although energy dissipation devices have been widely used for protecting structures since 1990 due to their low cost and efficiency, they still have some disadvantages. For example, displacement-dependent devices are not effective for small vibrations due to their high elastic stiffness [19,20]. Velocity-dependent devices such as viscoelastic dampers have a limitation in shear deformation capacity and there is a probability of tearing in elastomeric layers due to increased shear strain. Moreover, viscous dampers suffer from potential fluid leakage problems [19]. Disadvantages are also associated with motion-dependent devices that are tuned to one of the modes of vibration. They also occupy a large portion of the volume of the structure and lead to increased structural elements size [21].

In order to improve the performance of PED systems and increase the efficiency of structures, several studies have been conducted and hybrid damping systems have been introduced. Kim et al. [22] proposed a hybrid damping system that consists of a buckling restrained brace and a viscoelastic damper which is effective for controlling vibrations caused by wind and earthquakes in tall buildings. Moreover, Marshall et al. [23] conducted a numerical study to evaluate the performance of hybrid passive control devices that consist of a buckling restrained brace and either a high-damping rubber damper or viscous fluid damper in steel structures for two seismic hazards. In order to improve the performance of steel shear walls, diagonal and inverted V braces used as energy dissipation systems, Yamamoto and Son [20] proposed hybrid damping systems that combined them with viscoelastic damper. Also, Lee et al. [24] investigated hybrid dampers that are composed of friction dampers and steel slit dampers. Later on, Kim et al. [25] evaluated a 15-story reinforced concrete apartment building that was retrofitted with slit-friction hybrid dampers. Control of structures against seismic loads and provision of comfort for people on the top floors against wind vibrations are essential tasks given the fact that the inherent damping ratio of structures decreases with increasing height. Hence, Montgomery [26] proposed a fork configuration damper which could be used instead of coupling beams in coupled shear walls. The fork configuration damper consists of viscoelastic damper with reduced beam section (RBS) connection that has been evaluated under multiple levels of vibration. Moreover, researchers have conducted several studies to evaluate the combination of PED systems with semi-active/active control systems in order to reduce the wind and seismic response of structures [2,27,28].

Based on the above review of literature, hybrid damping systems are classified into two main categories: (a) Combination of PED devices with semi-active/active systems e.g. base isolation with an active or semi-active control actuator or tuned mass dampers with an active or semi-active control actuator [29,30]. (b) Combination of two or more energy dissipation devices. In this case, displacement and velocity dependent devices can be combined in parallel or series. In a parallel system, a similar relative displacement occurs in both dampers and as a result both dampers require a significant amount of deformation. Also, the stiffness of the HD increases and causes the performance of velocity-dependent device to decrease. Therefore, one may conclude that the velocity-dependent device is not effective for weak vibrations, while the combination can be effective for strong vibrations [20]. In a series system, a similar force occurs in both dampers and the displacement that occurs in each of the element causes dissipation of the input energy to the structure based on the distribution of stiffness. Therefore, this kind of HD system can be effective for weak vibrations [20].

In order to resolve the limitations of VED and MD, a new type of HD is proposed in this study, which is also appropriate for multi-level vibration control. In fact, the functional mechanism of this damper is such that the input energy is dissipated through shear in the elastomeric material and in-plane flexural yielding in the strips. Initially, strips of MDs were designed to prevent strain localization and early failures. Then, the dimensions and type of elastomeric layers were designed based on the elastic strength of strips. Three specimens were manufactured and tested cyclically to evaluate multi-phase performance. Finally, the finite element model (FEM) was constructed and analyzed in order to assess the behavior of the strips and HD. The simulation results were compared with the results obtained from the experiments.

2. Description of the proposed hybrid damper system

2.1. *Concept and mechanism of operation*

The configuration of the proposed HD is shown in Fig. 1. It consists of flexural yielding strips that are connected in parallel to each other and then connected vertically to a VED via a connection link (CL). The slotted holes on the connection link allow control of maximum range of displacement of the VED. The stoppers that connect the VED to the slotted holes of CL prevent tearing of viscoelastic layers due to large

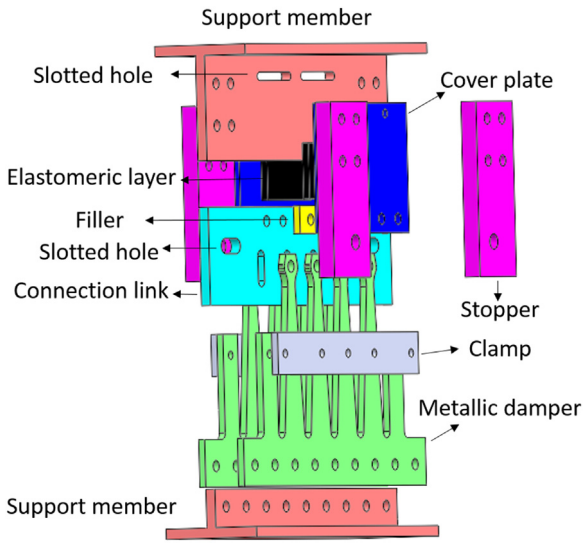

Fig. 1 – Configuration of the proposed HD.

deformations. This HD can be installed between a chevron brace and floor beam by T-shape sections of support members.

In general, it should be stated that the main function of the proposed HD is that it can partially mitigate the limitations associated with the VED (i.e. limited deformation capacity) and the MD (i.e. limited level energy dissipation capacity for small deformations). Also, the lock-up system and the use of clamps make it possible to use the maximum capacity of each of the dampers in the proposed HD. Moreover, the series connection between these dampers makes the proposed system effective for multi-level vibrations and results in multi-phase behavior. Fig. 2 shows the behavior of the HD and the ideal hysteresis curve.

Therefore, under weak earthquake and strong wind loads, phase I is anticipated, in which the VED dissipates energy through shear deformation and transforming vibrational energy into heat due to the internal friction between polymer chains, while the metallic yielding damper remains elastic and does not contribute to energy dissipation. Under strong seismic loads, phase II is anticipated for dissipating energy. In this phase, when the horizontal displacement reaches the maximum displacement amplitude of the VED, the mechanical stoppers will function and the range of displacement of the VED is restrained to prevent tearing of the elastomeric layers. Thus, the rest of the horizontal displacement is transmitted to the MD and the metallic damper functions and dissipates energy through in-plane flexural yielding. In this case, the efficiency of energy dissipation significantly increases compared to phase I because the MD provides energy dissipating capacity. In summary, the concept of the proposed HD can be presented as follows:

- The maximum displacement of the VED should be determined in such a range that the MD remains elastic. VED should be able to dissipate energy for small to moderate levels of vibration.
- The maximum displacement of the VED should be limited to a range that no tearing can occur in the elastomeric layers that are bonded between the steel plates.
- The activation load in the HD system should function in the strong range of vibrations. Hence, the maximum displacement of the VED should be restricted in strong vibrations, where the MD should dissipate energy through inelastic deformations.
- Stoppers must be strong enough and be able to resist the ultimate strength of the HD.

The hybrid damper can be modeled using the Kelvin–Voigt model (KVM) for the VED and a spring for MD that are connected to each other in series (Fig. 2a). In the frequency domain, the damping force of the viscoelastic damper F_{VE}, can be expressed using the elastic stiffness K_{VE}, and viscous damping coefficient C_{VE}, as follows [31]:

$$F_{VE}(\omega) = (K_{VE} + C_{VE}\omega_{VE}\mathrm{i})\tilde{u}_{VE}(\omega) \tag{1}$$

$$C_{VE} = 2m_{VE}\omega_{VE}\xi_{VE} \tag{2}$$

$$\omega_{VE} = \sqrt{K_{VE}/m_{VE}} \tag{3}$$

where m_{VE}, ω_{VE}, ξ_{VE} and i are mass, oscillating circular frequency, damping ratio and imaginary unit, respectively. By substituting Eqs. (2) and (3) in Eq. (1), the force of the VED is equal to:

$$F_{VE}(\omega) = (K_{VE} + 2K_{VE}\xi_{VE}\mathrm{i})\tilde{u}_{VE}(\omega) \tag{4}$$

The relationship between the damping force of the metallic damper F_M, and displacement u_M, is as follows:

$$F_M = K_M u_M \tag{5}$$

where K_M is the stiffness of the metallic yielding damper. Since the connection of the two dampers are in series, the equivalent stiffness of hybrid damper K_{HD}, is calculated as follows [20]:

$$1/(K_{HD}(1 + 2\xi_{HD}\mathrm{i})) = 1/(K_{VE}(1 + 2\xi_{VE}\mathrm{i})) + 1/K_M \tag{6}$$

$$\begin{aligned} K_{HD}(1 + 2\xi_{HD}\mathrm{i}) &= \frac{1}{\frac{K}{VE} - \frac{2K_{VE}\xi_{VE}\mathrm{i}}{K_{VE}^2 + (2K_{VE}\xi_{VE}\mathrm{i})^2} + \frac{1}{K}} \\ &\approx \frac{1}{\frac{1}{K} - \frac{2\xi_{VE}\mathrm{i}}{K} + \frac{1}{K}} = \frac{K_M K_{VE}}{K_{VE} + K_M(1 - 2\xi_{VE}\mathrm{i})} \\ &\approx \frac{K_M K_{VE}}{K_{VE} + K_M} + \frac{2K_M K_{VE} K_M \xi_{VE}\mathrm{i}}{(K_{VE} + K_M)^2} \end{aligned} \tag{7}$$

$$k = K_M/(K_{VE} + K_M) \tag{8}$$

$$\begin{aligned} K_{HD}(1 + 2\xi_{HD}\mathrm{i}) &= kK_{VE}(1 + 2k\xi_{VE}\mathrm{i}) \\ &= (K_M K_{VE}(1 + 2\xi_{VE}\mathrm{i}))/(K_M + K_{VE}(1 + 2\xi_{VE}\mathrm{i})) \end{aligned} \tag{9}$$

In general, the stiffness of the VED is equivalent to or lower than the stiffness of the MD. Therefore, the minimum value of k is 0.5. On the other hand, the damping ratio of the VED under severe frequency is equal to 15–20%. In addition, the stiffness and damping ratio of the HD are k times that of the VED. Thus, we can design the damping ratio of the HD at least between 8% and 10%.

2.2. *Design approach and recommended details*

In order to fulfill the desired objectives of the proposed HD, the main point is that the restoring force of the VED for the target maximum displacement in VED must be less than the elastic strength of the MD. The elastic strength and elastic stiffness of strips may be calculated by numerical modeling. Then, the dimension and number of elastomeric layers can be determined based on the type of compound. On the other hand, the geometric shape of the flexural yielding strips must be designed such that no concentric stress may occur across the height of the strips. When the strips of the metallic yielding damper are subjected to in-plane shear load, V, bending moment and shear force simultaneously occur in individual strips of the damper. Therefore, this MD can dissipate energy

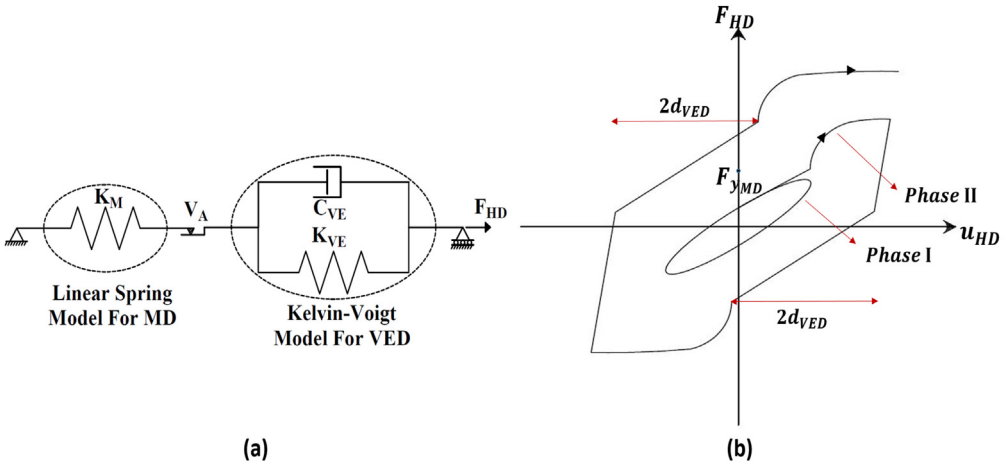

Fig. 2 – Combined behavior of HD specimen: (a) numerical modeling and (b) idealized hysteresis curve.

through shear and in-plane bending yielding of its strips. The proposed metallic yielding damper is composed of several strips that act in parallel. Therefore, the lateral force resisted by each strip is equal to:

$$v = V/n \tag{10}$$

where v and n are the lateral shear force that is applied to a strip and the number of strips, respectively. Steel strips of SSD [32] and CTD [7] can be modeled as a fixed beam at both ends with differential support movement (Fig. 3). Therefore, the moment distribution behavior of CTD is half that of the SSD behavior. Thus, the amount of moment over the height of the strip may be computed as follows:

$$M_x = (\alpha M_1 x)/h = vx \tag{11}$$

where M_1 and h are the maximum moment at the ends and the height of the strip, respectively. It should be noted that α is the coefficient associated with the type of strip. It is equal to 2 and 1 for SSD and CTD strips, respectively. Also, the plastic moment is equal to:

$$M_{p,x} = F_y Z_x = F_y((t_x b_x^2)/4) \tag{12}$$

where F_y, Z_x, t_x and b_x are yield stress, plastic section modulus, thickness and width of the strip, respectively. Since the aim of designing the strips is achievement of plastic yielding, Eqs. (11) and (12) can be used to obtain the following:

$$b_x = 2(vx/(F_y t_x))^{0,5} = 2\lambda\sqrt{x} \tag{13}$$

where λ is the strip shape coefficient. Therefore, the shape of the strips should be a parabolic one. In order to prevent premature shear failure, the minimum width of the strip must be larger than that given by Eq. (14) [32].

$$b_0 > (2\sqrt{3}v)/(F_y t_0) \tag{14}$$

where t_0 is the thickness of the strip at the middle and end of the strip in SSD and CTD, respectively. Assuming that the shape factor (i.e. plastic section modulus to elastic section

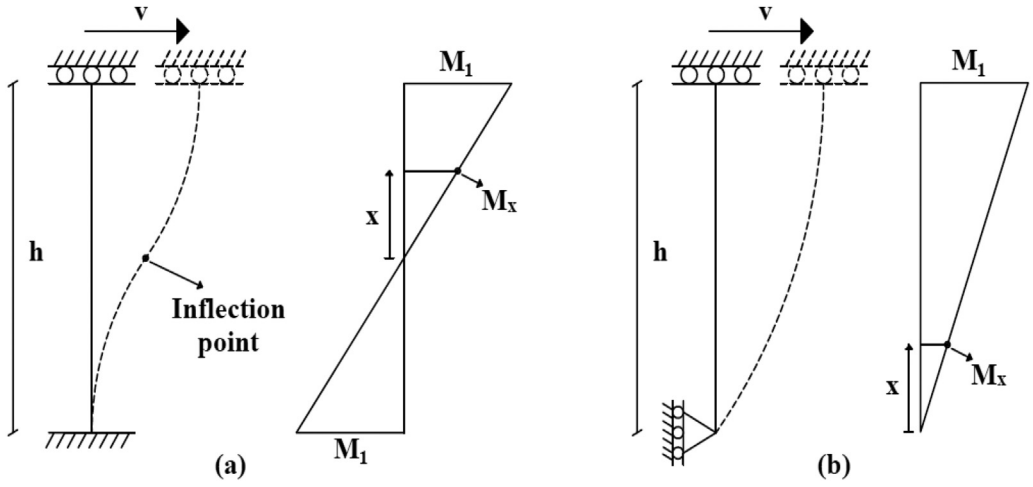

Fig. 3 – Deformed shape and bending moment model for strips: (a) SSD and (b) CTD.

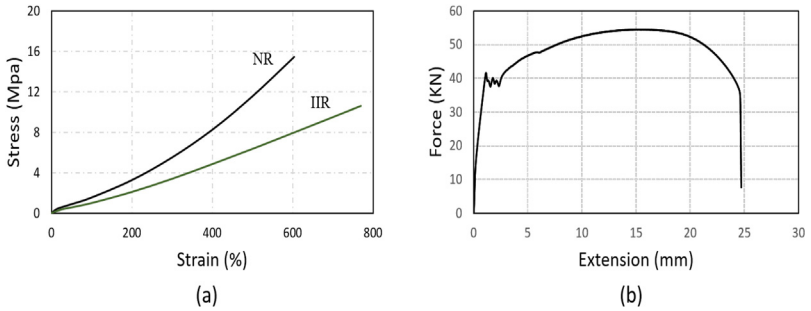

Fig. 4 – Tensile test: (a) stress–strain curve for NR and IIR and (b) force-extension for steel.

modulus ratio) is equal to 1.5 for a rectangular shape, the yielding strength is as follows based on Eqs. (11) and (12):

$$P_y = (\alpha F_y t_x b_x^2)/6h = (2/3)F_y t_x \lambda^2 \tag{15}$$

The virtual work method can also be used to calculate the elastic displacement and stiffness of metallic dampers.

$$1\times\delta = \int (M_x m_x)/(EI_x)dx = 12\alpha P/E\int_0^{(h/\alpha)} (x^2/(t_x b_x^3))dx \tag{16}$$

where E, I_x are Young's modulus and moment of inertia at location x, respectively.

$$K_e = cP/\delta = cE/(12\alpha\int_0^{h/\alpha}(x^2/(b_x^3 t_x))dx) = c(Et\lambda^3)/(\alpha(h/\alpha)^{1.5}) \tag{17}$$

where c is the stiffness calibration coefficient that is less than 1 [33]. However, with decreasing the rigidity at both ends of the strip, this coefficient decreases.

3. Test program

3.1. *Material properties*

3.1.1. *Elastomeric material*

VEDs are mainly made with elastomeric materials that are vulcanized between steel plates under pressure and heat with suitable adhesives. This type of material shows hyperelastic and time-dependent behavior that is known as viscoelastic material. The time-dependent behavior of VEDs will be discussed later. In order to evaluate hyperelastic properties of the elastomeric material, tensile tests were carried out on tension coupons based on ASTM D412 [34]. Fig. 4a shows the stress–strain response of the elastomeric materials based on NR and IIR.

3.1.2. *Steel*

In order to evaluate the mechanical properties of the steel plates, tensile tests were conducted on steel dogbone specimens based on ASTM A370 [35]. The tension coupons were cut from the same material that was used in the construction of MDs by using a water jet machine. Fig. 4b shows the force-extension response of the steel coupon specimen.

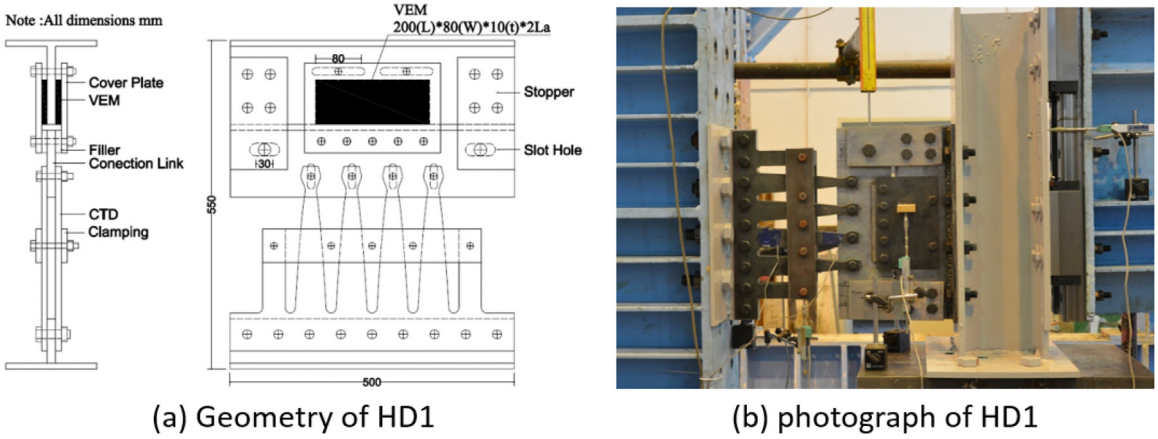

Fig. 5 – Specimen HD1.

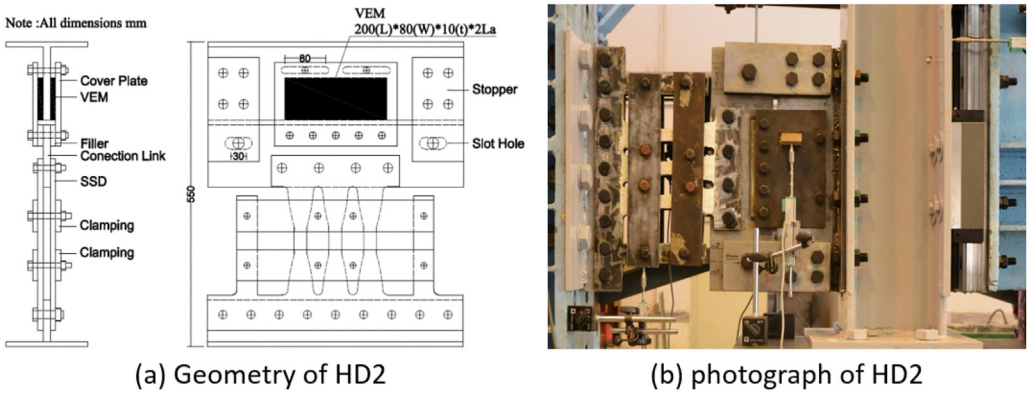

Fig. 6 – Specimen HD2.

3.2. *Construction and assembling of the specimens*

In this study, three specimens were manufactured with different geometrical strips, elastomeric compounds and loading protocols. Initially, two HD specimens were manufactured as follows: (a) HD1 composed of CTD and VED based on NR compound (b) HD2 composed of SSD and VED based on IIR compound. Figs. 5 and 6 show the details and dimensions of the HD1 and HD2, respectively. Later, the third specimen (HD3) was fabricated similar to HD1 given the performance of the two previous hybrid dampers, i.e. the appropriate shear displacement capacity of HD1. The main difference between HD1 and HD3 was the loading protocol used for the tests, that will be discussed later.

Fig. 7 – VED specimen.

The metallic parts of the HD, including CTDs and SSDs were made of ST37 steel plates with a thickness of 10 mm by water jet cutting. The main purpose of using this method of cutting is its high accuracy, which prevents generation of residual stress. The height to width ratio of the strips (i.e. aspect ratio) was set equal to 4.5 and 4.2 for CTD and SSD, respectively in order to have dominant flexural behavior in the strips of the MDs. Moreover, a pair of clamps were used to restrain out-of-plane deformation and prevent local buckling in each of the strips. Afterwards, two elastomeric layers with dimension of $80 \times 200 \times 10$ mm were vulcanized and adhered between the support member and the two steel plates (Fig. 7). Then, the connection link was used to connect them with high-tension bolts (HV10.9), so that the maximum displacement of VED was controlled by stopper bolts (HV12.9). It should be noted that the maximum shear deformation of the VED was restricted to 150% and the diameter of stopper bolts was 22 mm. The main objective of using high-tension bolts instead of welding is that it is an easy method for assembling the elements, eliminates the uncertainties caused by welding and prevents damage in the elastomeric layers. In addition, the bolts were fastened with lock nuts in order to prevent the bolts from falling off and losing the pre-stress under cyclic loading. It should be noted that when the VED and MD are assembled together, the pre-tension that occurs in the bolts results in undesirable debonding between the elastomeric layers and the steel plates. Therefore, two slotted holes are fabricated on the support member that are longer than the maximum shear displacement of VED and their sole function is to restrain the cover plates and support member from out of plane displacement.

3.3. *Test setup*

Fig. 8 shows the designed test setup. As seen, the test setup consists of a 50 ton vertical actuator and reaction frames that are mounted on the strong floor. Then, a short loading column with four linear bearings is placed on the actuator and load cell

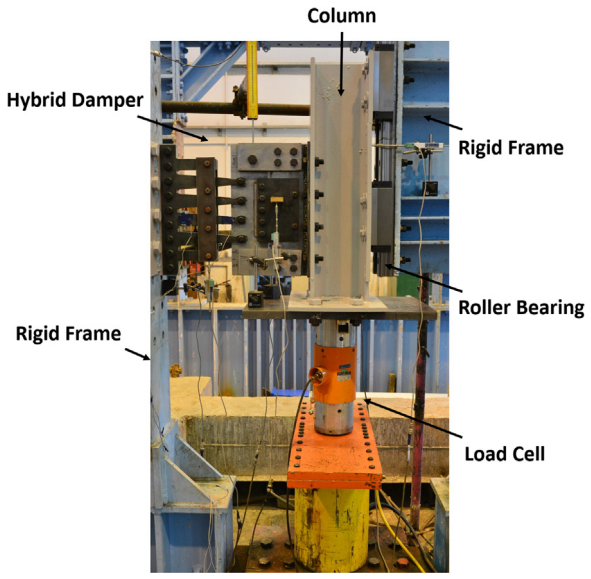

Fig. 8 – Test setup.

in such a way that one side of the flange of the short loading column with roller bearings is connected to the reaction frame. Afterwards, the test specimens are installed between the short loading column and the reaction frame. Finally, a displacement-controlled loading protocol is applied to each HD specimen quasi-statically. The main purpose that linear bearings were employed between the reaction frame and the short column is to prevent the short column from out-of-plane deformation and damage to the loading device. Moreover, a set of LVDTs were positioned to measure the relative VE and MD displacement and also the out-of-plane displacement of one strip.

3.4. *Loading protocol*

The test specimens were subjected to the following sequence of fully reversed sinusoidal cyclic loading according to ASCE7-16 [36]. Three stages of displacement-controlled cyclic loading designed to evaluate the performance of HD, were applied to the specimens. The first stage is designed to investigate the performance of VED (Phase I) and the second and third stages are meant to evaluate the performance of the combined behavior (Phase II) of HD given that the target maximum displacement amplitude of MD is considered equal to 40 mm and 60 mm for each of the stages, respectively. It should be noted that the third stage of the loading protocol is to investigate maximum shear displacement capacity in HD, while no failures occur in the second stage. Based on the maximum shear displacement of VED, a cyclic loading including displacement amplitudes of 1, 3, 5, 7, 10, 15 mm with 3 number of cycles for phase I were conducted. Thus, the metallic damper must tolerate ten, five and three cycles corresponding to 0.33, 0.67 and 1 times the target maximum displacement amplitude according to ASEC7-16 loading protocol. The loading protocol is shown in Fig. 9. The main difference between HD1, HD2 and HD3 is the target maximum displacement of MD, so the target maximum displacement of HD3 is considered based on two previous specimens and without increasing it.

4. Test results

4.1. *Hysteresis response*

The force–displacement hysteresis curves for the first and second specimens are shown in Figs. 10 and 11, respectively. The figures clearly show the multi-phase behavior of each of the components under the set of loads in the loading protocol. The experimental results indicate stable hysteric behavior without any sudden degradation in strength and stiffness and

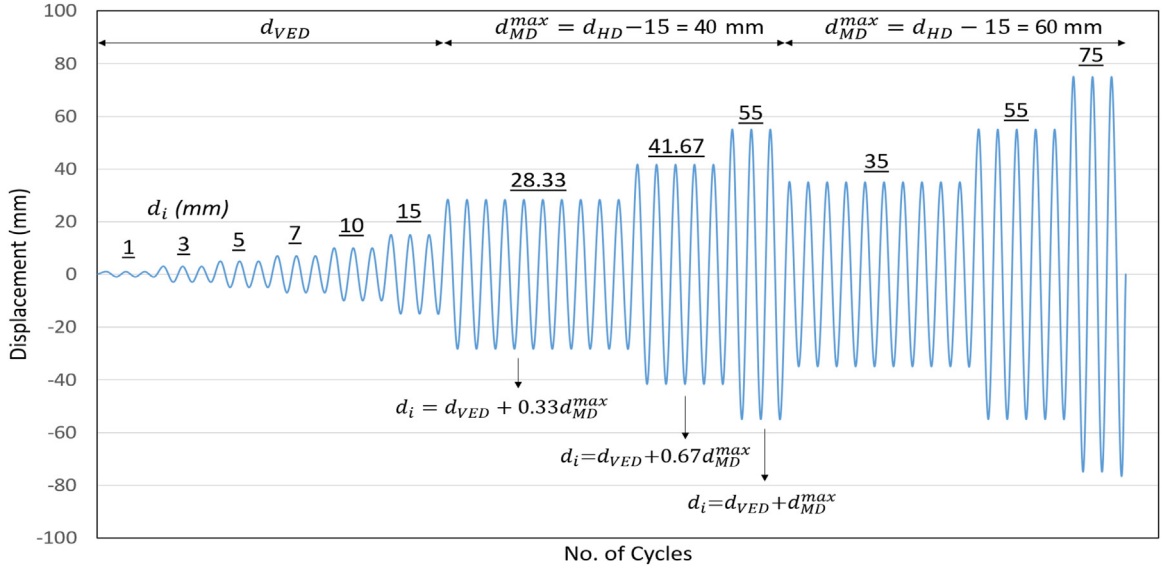

Fig. 9 – Cyclic loading protocol for HD specimens.

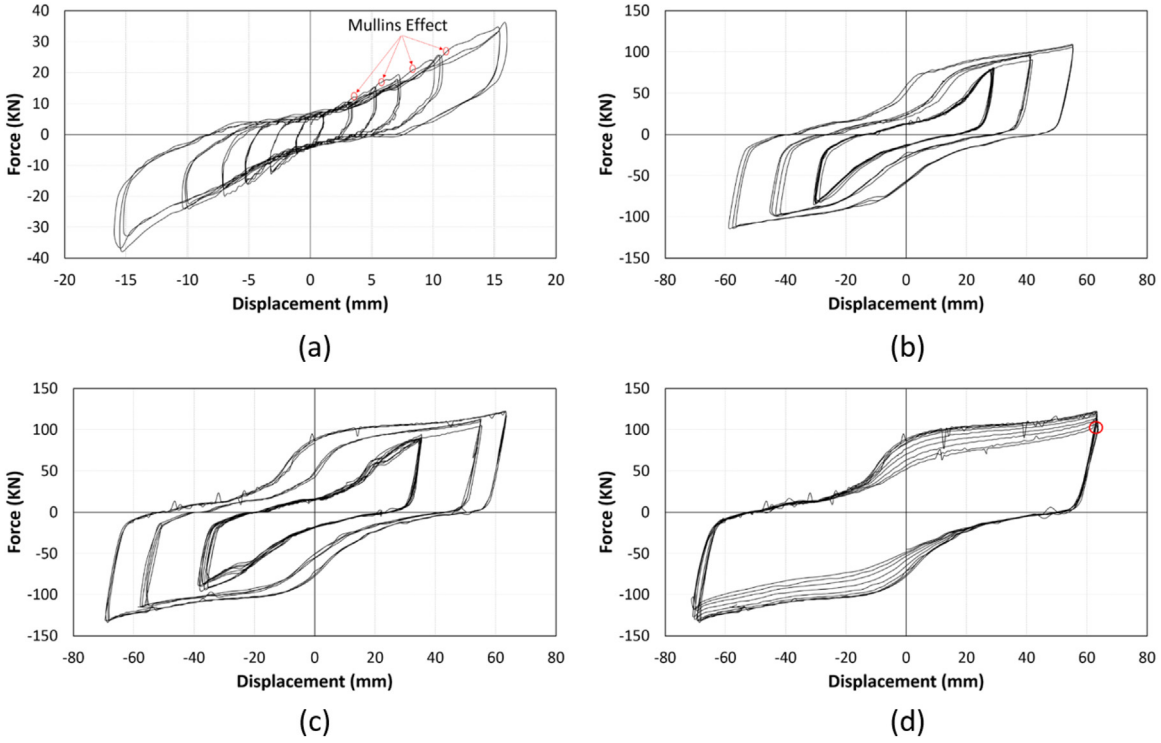

Fig. 10 – Hysteresis curves of HD1: (a) phase I, (b) phase II with the maximum displacement of 40 mm for CTD, (c) phase II with the maximum displacement of 60 mm for CTD and (d) repeat the last cycle.

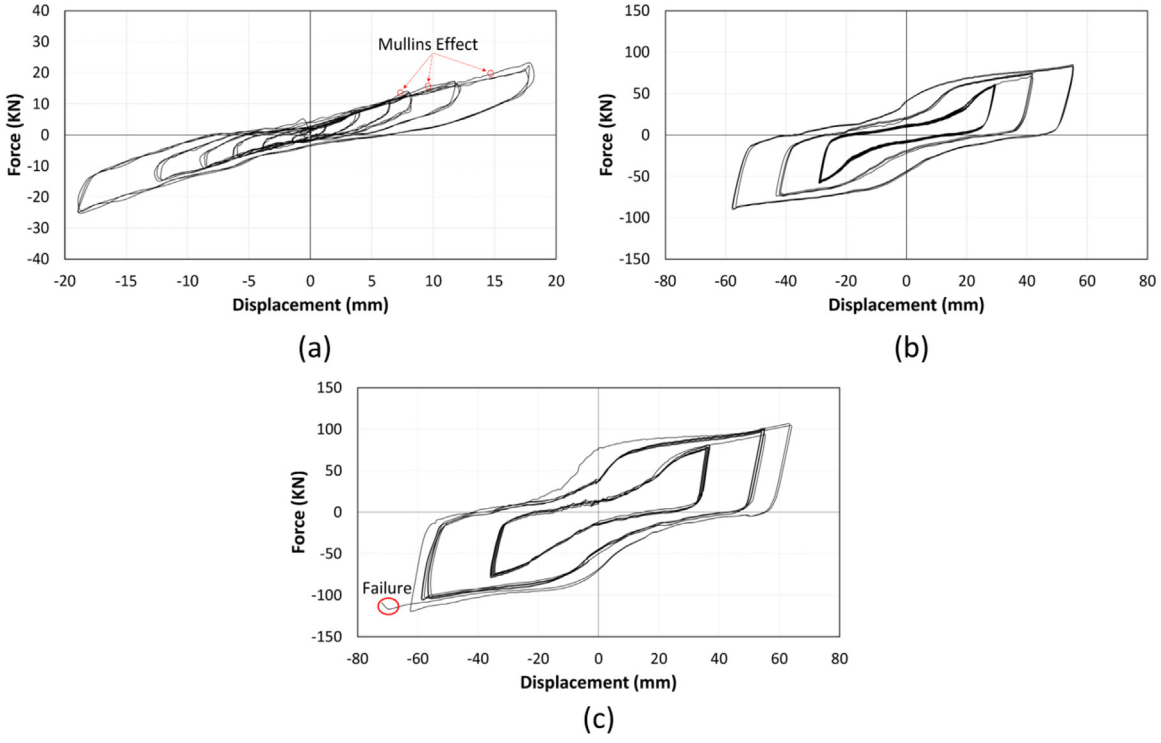

Fig. 11 – Hysteresis curves of HD2: (a) phase I, (b) phase II with the maximum displacement of 40 mm for SSD and (c) phase II with the maximum displacement of 60 mm for SSD.

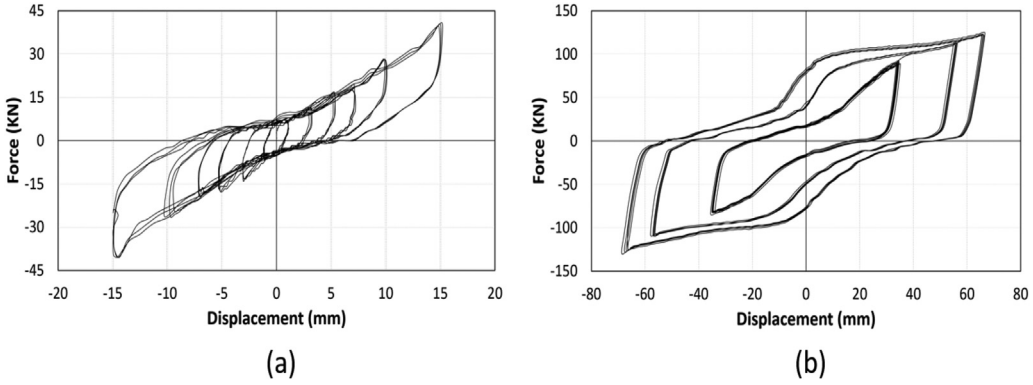

Fig. 12 – Hysteresis curve of HD3: (a) phase I, (b) phase II with the maximum displacement of 60 mm for CTD.

appropriate energy dissipation capacity for multi-level vibrations. VED in phase I has sufficient damping as seen in Figs. 10a and 11a. It can be observed that the damping capacity for the displacement range of 15 mm of VED is at least 10% while the displacement range of CL was measured by LVDT3 to be less than 2 mm. This indicates that in this phase the MDs remain elastic and do not provide any damping capacity. It should be noted that damping capacity goes up with increasing rate of loading or decreasing displacement of VEDs, which will be discussed later. Also, the rate of variation of damping is different depending on the type of elastomeric compound. In the first cycle after an increase in displacement, there is a reduction in strength in phase I. The main reason for this is the Mullins effect by which the softening phenomenon occurs at the beginning of deformation cycles due to breaking of weak bonds.

Given target maximum displacement of 40 mm for MDs, the hysteresis curves for two specimens in phase II loading protocol are shown in Figs. 10b and 11b. Since the hysteresis behavior was completely stable for two specimens and no failures occurred in the strips and there was no degradation in strength, the target maximum displacement was increased to 60 mm and they were loaded cyclically according to Section 3.4 (Figs. 10c and 11c). At the end of the loading protocol, the HD1 specimen could still dissipate energy because there were no evidence of cracking, failure or reduction of strength of the strips or the elastomeric layers. Therefore, the last cycle of the cyclic loading was repeated and after completion of the protocol considered in Section 3.4, seven cycles with a range of 75 mm were applied. After the 5th cycle at this amplitude, the strength of HD1 began to reduce as seen in Fig. 10d. Finally, the cyclic test was stopped at the 7th cycle of the same amplitude because the maximum and minimum strength at zero displacement decreased as much as 15% while there were no cracks or failures in HD1. However, at the beginning of the loading protocol for the second specimen HD2 with 75 mm displacement, one of the strips of the MDs failed (Fig. 11c). Since HD1 could tolerate more cycles in comparison with HD2, the third specimen, HD3 was constructed similar to HD1 with a slight modification. In this specimen, a steel plate was placed between the two layers of MDs and then three clamps were attached to each other by high strength bolts. The main objective of this is to prevent the teeth from moving toward each other that was observed in the cyclic test of HD1. Fig. 12 shows the hysteresis behavior of the third specimen, HD3, in phase I and phase II.

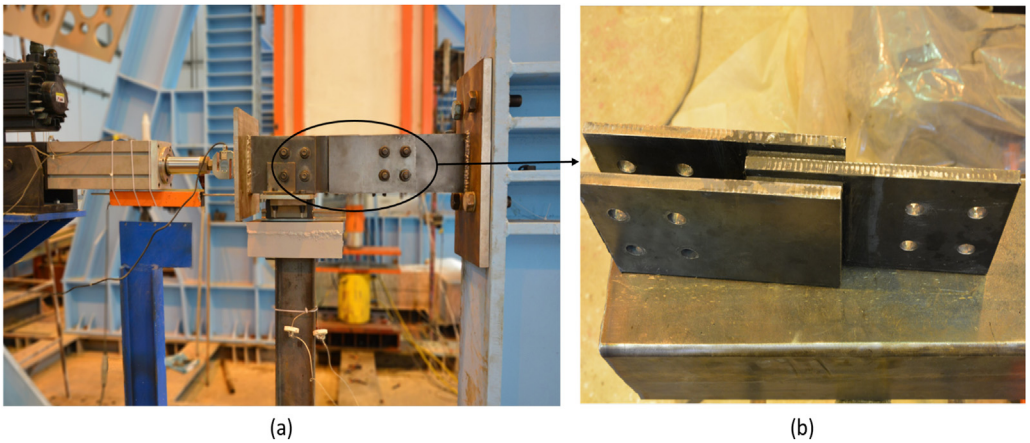

Fig. 13 – Experimental test: (a) test setup and (b) VED specimen.

Table 1 – Loading protocol for VED.

Freq.	Strain%						Number of cycles
	Test1	Test2	Test3	Test4	Test5	Test6	
0.1	10	30	50	70	100	150	15
0.2	10	30	50	70	100	150	15
0.3	10	30	50	70	100	150	15
0.5	10	30	50	70	100	150	15
1	10	30	50	70	100	150	15
1.5	10	30	50	70	100	150	15

4.2. *Equivalent damping of VEDs*

In order to evaluate the dynamic properties of VEDs, small scale samples of VEDs were manufactured and subjected to sinusoidal excitations. Fig. 13 illustrates the VED specimens and the test setup used. Since elastomeric materials are dependent on strain and strain rate, a test program with different frequency and strain was designed. Based on previous research [13,37,38], the material tests were designed to obtain the mechanical properties of the VED under loading conditions that may occur under low-to-strong earthquakes. Table 1 shows the cyclic loading tests. This test program involves shear strain range between 10% and 150% and frequency between 0.1 and 1.5%Hz.

The experimental results show a stable hysteresis behavior with high energy dissipation, Therefore, the Kelvin–Voigt modeling (KVM) technique is utilized to define the behavior of viscoelastic dampers considering the experimental results and the hysteresis curves that are approximately in the form of full ellipse. Damping capacity $\eta/2$, and stiffness coefficients K_S, of the VEDs may be obtained as follows:

$$\eta = G_L/G_S = F_2/F_1 = \tan\theta \tag{18}$$

$$K_S = F_1/u_0 = (n_{VE}G_S A)/h \tag{19}$$

where G_S is shear storage modulus and G_L is shear loss modulus. n_{VE}, h, A are number, thickness and shear area of the viscoelastic layers, respectively.

Fig. 14 shows the dynamic parameters of VED based on NR and IIR. The results show that the equivalent damping ratio of VEDs based on IIR is at least 15% while the equivalent damping ratio of VE damper based on NR is 13%. However, the main difference between NR and IIR viscoelastic dampers is that the latter has more damping capacity, while the former has a higher stiffness.

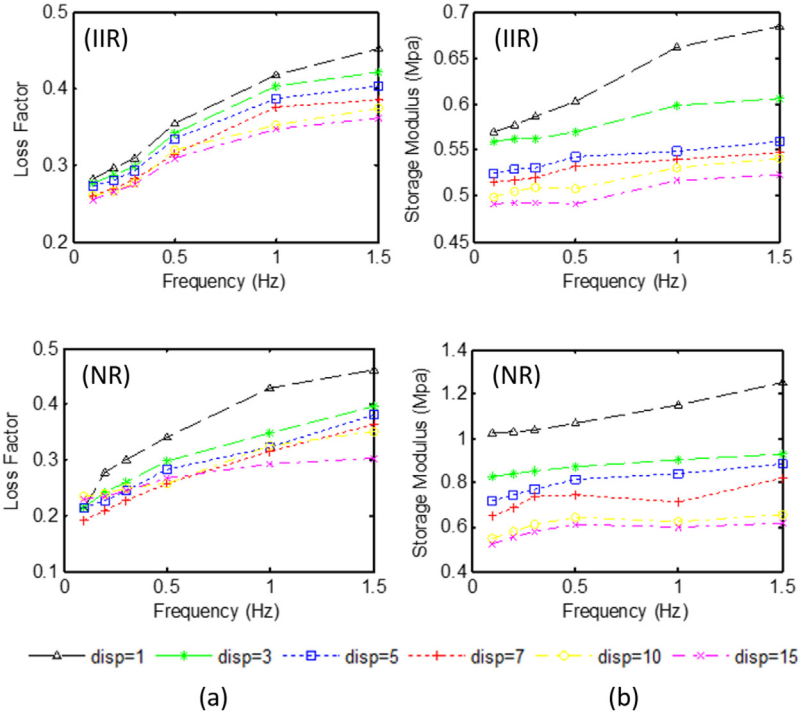

Fig. 14 – Dynamic parameters for IIR and NR viscoelastic damper: (a) loss factor and (b) storage modulus.

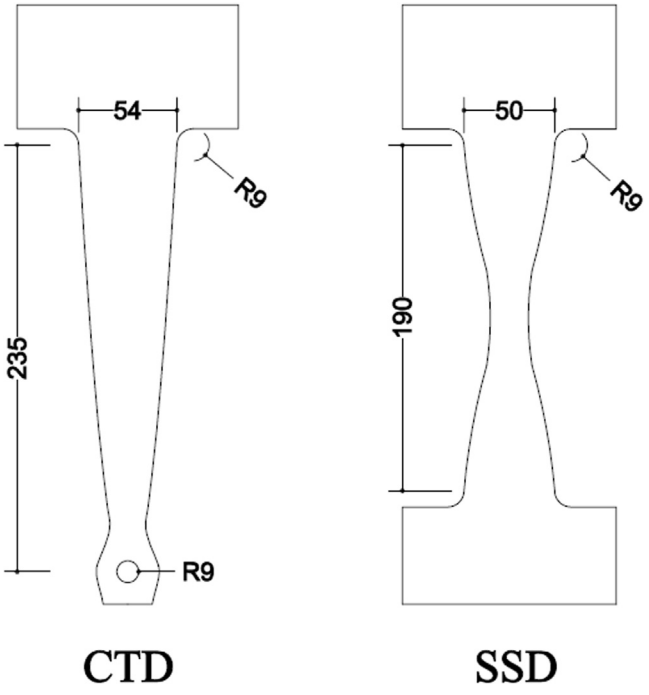

Fig. 15 – The geometry of an individual strip.

5. Numerical study

5.1. *Finite element modeling*

In order to simulate and predict the behavior of HD, the finite element method (FEM) and ABAQUS software [39] has been used. Initially a single strip of MDs was modelled (Fig. 15) and its nonlinear behavior was investigated. Each of the strips was modeled using three-dimensional solid elements and quadratic reduced-integration elements (C3D20R). The data related to the tensile coupon test were used to define the linear and nonlinear behavior of steel strips. The engineering stress–strain results that were obtained from the coupon test were first converted to true stress–strain information by using the following equation.

$$\sigma = P/A \tag{20}$$

$$\varepsilon = Ln(A_0/A) \tag{21}$$

where A_0 and A are the initial and current section area of the specimen, respectively. The isotropic-kinematic hardening model was used in order to take the hardening behavior of the strips into account. On this basis, it was assumed that the yield surface increases according to the following equation:

$$\sigma = \sigma_0 + Q_\infty(1-e^{-b\varepsilon_p}) \tag{22}$$

where σ_0 and ε_p are the initial yield stress and equivalent plastic strain, respectively. Also, Q_∞ and b are the material parameters. It should be noted that the calibrated values of the model for the strip of steel sample, including σ_0, Q_∞ and b are equal to 285 MPa, 50 MPa and 5, respectively.

Three-dimensional solid reduced-integration hybrid continuum elements (C3D20HR) were used in modeling elastomeric layers. The hyperelasticty of the VE material was obtained from tensile test that are characterized by different forms of strain-energy density functions, w, and can be calculated as follows:

$$\partial W = \int \sigma_{ij}\partial\varepsilon_{ij}d\upsilon \tag{23}$$

where W, σ_{ij} and ε_{ij} denote the stored strain energy per unit reference volume (v), the components of stress and strain tensors, respectively. Moreover, time-dependent behavior can be investigated by using creep and stress relaxation tests. Therefore, a relaxation test was carried out under constant 30% shear strain for under 250(s) for the NR viscoelastic damper in order to simulate the VED in FE software. Then, the software calculates the prony series coefficients by using the following:

$$g_R(t) = 1-\sum_{i=1}^{N} g_i(1-e^{-t/\tau_i}) \tag{24}$$

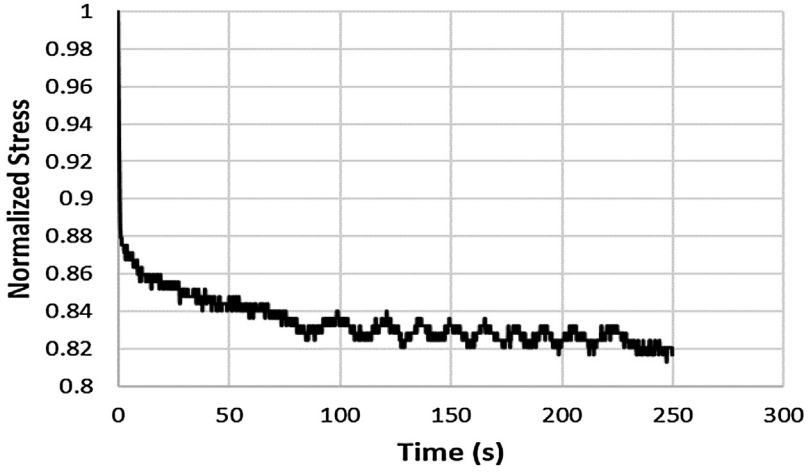

Fig. 16 – Relaxation test response for the VED based on NR.

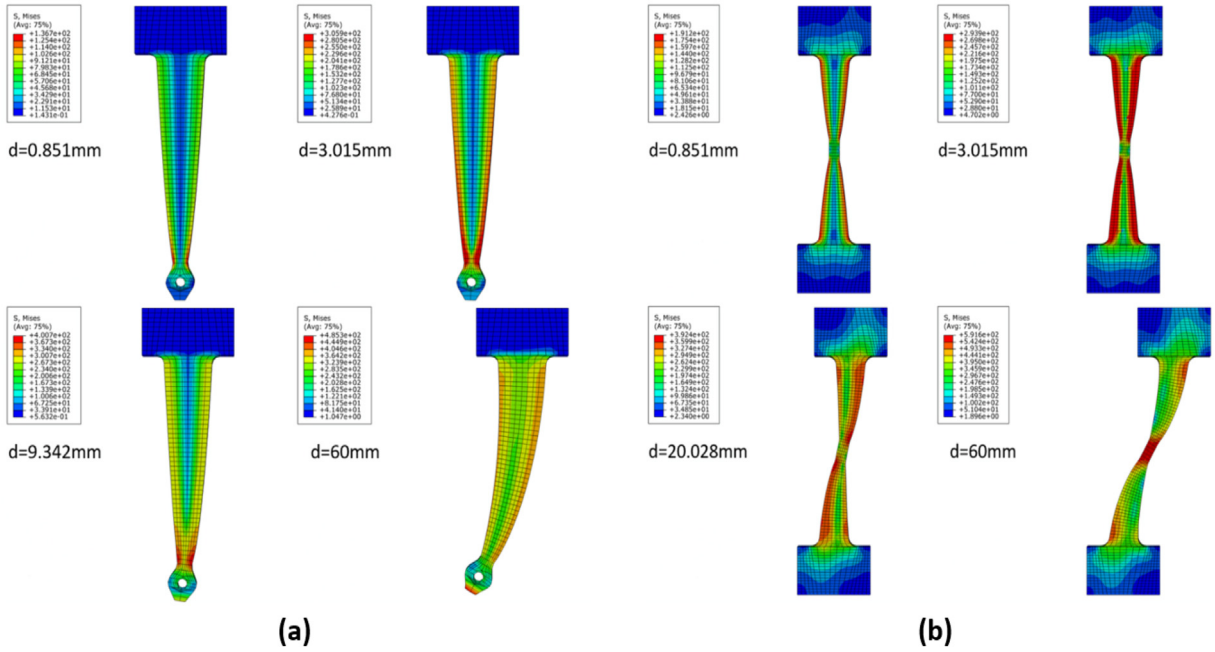

Fig. 17 – Stress distribution over the height of strips in different stages of displacement loading: (a) Von-Mises stress of CTD and (b) Von-Mises stress of SSD.

Table 2 – Elastic parameters of studied strips.

		P_y (N)	K_e (N/mm)	δ_y (mm)
CTD	Analytical equations	5889	3005	1.96
	Finite element model	5709	2869	1.99
SSD	Analytical equations	5945	5945	1
	Finite element model	6007	6390	0.94

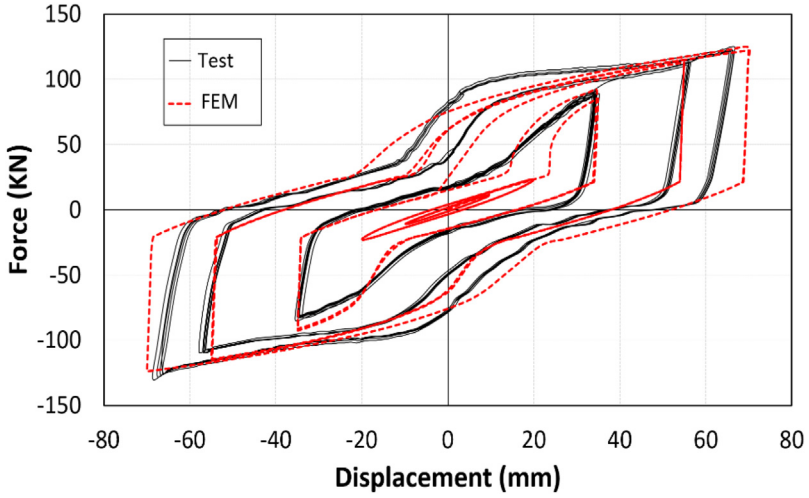

Fig. 18 – Comparison of finite element hysteretic curve with test result of the HD3.

where g_R denotes the dimensionless shear relaxation modulus, and g_i and τ_i are constant parameters. Fig. 16 shows the variations of stress versus time.

5.2. *Numerical results*

Fig. 17 shows the stress contour plot for each type of strip. Plastic deformation with uniform distribution is completely observed over the height of strips as expected. Afterwards, the

yield strength, elastic stiffness and initial yield displacement were determined by monotonic loading and were compared with analytical equations. There is a good agreement between the results obtained as it can be seen in Table 2. Finally, the behavior of HD3 specimen was simulated using the FEM.

A comparison of results obtained from experimental tests and numerical simulation are shown in Fig. 18. It can be seen that the numerical simulation correctly predicts the multi-phase behavior of HD. In displacement ranges less than 15 mm (phase I), the metallic damper remains elastic and the numerical model shows that energy dissipation occurs by viscoelastic dampers. However, existing inaccuracies in installation of HDs and the attachment of screws to the ends of slotted holes in the displacement range less than the intended displacement range to activate the stoppers, are primary reasons that the experimental results show some difference with numerical simulations at displacement ranges more than 15 mm. Nevertheless, the overall agreement between the results may be considered satisfactory.

6. Conclusions

A new type of HD that consists of VED and MD is introduced in this study. In order to investigate the multi-phase behavior of HDs, three specimens were manufactured and tested under cyclic loading according to ASCE7-16. Analytical equations and numerical simulations were used in the design of the specimens and then the results were compared with those of experimental tests. The main results from this research may be summarized as follows:

The series connection of VED and MD using fuse system leads to prevent tearing elastomer layers under strong vibrations. VED can dissipate energy for weak level vibrations, while the MDs remain elastic. But, both dampers can dissipate energy under strong vibration. Experimental results confirmed proper multi-phase performance.

At small vibration levels, the VED specimens had a damping ratio higher than 10%, which is provided by elastomeric layers. Generally damping in VED specimens show a significant dependence on strain amplitude and excitation frequency. However, the dependency of VED on strain amplitude and excitation frequency based on NR is more remarkable than that of VED based on IIR.

The experimental results show that special geometry of metallic strips and the use of special clamps to restrain out-of-plane buckling of strips cause the ductility of strips to increase. The HD based on CTD showed 75 mm shear displacement capacity, while the HD based on SSD showed 55 mm shear displacement capacity.

The analytical equations for designing the geometry of strips show that there is a good correlation with numerical simulations in such a way that uniform stress distribution over the height of the strips is guaranteed. Also, the FEM could correctly predict the behavior of HD.

The cyclic loading tests showed that the proposed HDs possess stable hysteretic behavior and high energy dissipation capacity. Therefore, it can be used as a fuse mechanism for dissipating the input seismic energy in structures.

Conflict of interest statement

The authors hereby declare that in carrying out this research and publishing the results, they have no conflict of interest.

REFERENCES

[1] T.T. Soong, G.F. Dargush, Passive Energy Dissipation Systems in Structural Engineering, John Wiley and Sons, 1997.
[2] T.T. Soong, B.F. Spencer Jr., Supplemental energy dissipation: state-of-the-art and state-of-the-practice, Eng. Struct. 24 (2002) 243–259.
[3] F.Y. Cheng, H. Jiang, K. Lou, Smart Structures: Innovative Systems for Seismic Response Control, CRC Press, 2008.
[4] G.D. Ashkezari, A.A. Aghakouchak, M. Kokabi, Design, manufacturing and evaluation of the performance of steel like fiber reinforced elastomeric seismic isolators, J. Mater. Process. Technol. 197 (2008) 140–150.
[5] M.C. Constantinou, T.T. Soong, G.F. Dargush, Passive Energy Dissipation Systems for Structural Design and Retrofit, 1998.
[6] A. Benavent-Climent, A brace-type seismic damper based on yielding the walls of hollow structural sections, Eng. Struct. 32 (2010) 1113–1122.
[7] S. Garivani, A. Aghakouchak, S. Shahbeyk, Numerical and experimental study of comb-teeth metallic yielding dampers, Int. J. Steel Struct. 16 (2016) 177–196.
[8] S. Mirzabagheri, M. Sanati, A. Aghakouchak, S. Khadem, Experimental and numerical investigation of rotational friction dampers with multi units in steel frames subjected to lateral excitation, Arch. Civ. Mech. Eng. 15 (2015) 479–491.
[9] C.J. Black, N. Makris, I.D. Aiken, Component testing, seismic evaluation and characterization of buckling-restrained braces, J. Struct. Eng. 130 (2004) 880–894.
[10] R. Tremblay, P. Bolduc, R. Neville, R. DeVall, Seismic testing and performance of buckling-restrained bracing systems, Can. J. Civ. Eng. 33 (2006) 183–198.
[11] E.J. Nielsen, M.L. Lai, T.T. Soong, J.M. Kelly, Viscoelastic damper overview for seismic and wind applications, in: Smart Structures and Materials 1996: Passive Damping and Isolation, vol. 2720, International Society for Optics and Photonics, 1996 138–145.
[12] Z.D. Xu, D.X. Wang, C.F. Shi, Model, tests and application design for viscoelastic dampers, J. Vib. Control 17 (2011) 1359–1370.
[13] Z.D. Xu, Y.X. Liao, T. Ge, C. Xu, Experimental and theoretical study of viscoelastic dampers with different matrix rubbers, J. Eng. Mech. 142 (2016) 04016051.
[14] D. Lee, D.P. Taylor, Viscous damper development and future trends, Struct. Des. Tall Build. 10 (2001) 311–320.
[15] J.J. Connor, Introduction to Structural Motion Control, Prentice Hall, 2003.
[16] M.M. Ali, K.S. Moon, Structural developments in tall buildings: current trends and future prospects, Arch. Sci. Rev. 50 (2007) 205–223.
[17] S.M. Zahrai, S. Abbasi, B. Samali, Z. Vrcelj, Experimental investigation of utilizing TLD with baffles in a scaled down 5-story benchmark building, J. Fluids Struct. 28 (2012) 194–210.
[18] N.B. Chancellor, M.R. Eatherton, D.A. Roke, T. Akbas, Self-centering seismic lateral force resisting systems: high performance structures for the city of tomorrow, Buildings 4 (2014) 520–548.
[19] M. Symans, F. Charney, A. Whittaker, M. Constantinou, C. Kircher, M. Johnson, R. McNamara, Energy dissipation

systems for seismic applications: current practice and recent developments, J. Struct. Eng. 134 (2008) 3–21.
[20] M. Yamamoto, T. Sone, Damping systems that are effective over a wide range of displacement amplitudes using metallic yielding component and viscoelastic damper in series, Earthq. Eng. Struct. Dyn. 43 (2014) 2097–2114.
[21] C. Christopoulos, M. Montgomery, Viscoelastic coupling dampers (VCDs) for enhanced wind and seismic performance of high-rise buildings, Earthq. Eng. Struct. Dyn. 42 (2013) 2217–2233.
[22] D.H. Kim, Y.K. Ju, M.H. Kim, S.D. Kim, Wind-induced vibration control of tall buildings using hybrid buckling-restrained braces, Struct. Des. Tall Special Build. 23 (2014) 549–562.
[23] J.D. Marshall, F.A. Charney, Seismic response of steel frame structures with hybrid passive control systems, Earthq. Eng. Struct. Dyn. 41 (2012) 715–733.
[24] C.H. Lee, J. Kim, D.H. Kim, J. Ryu, Y.K. Ju, Numerical and experimental analysis of combined behavior of shear-type friction damper and non-uniform strip damper for multi-level seismic protection, Eng. Struct. 114 (2016) 75–92.
[25] J. Kim, H. Shin, Seismic loss assessment of a structure retrofitted with slit-friction hybrid dampers, Eng. Struct. 130 (2017) 336–350.
[26] M.S. Montgomery, Fork Configuration Damper (FCDs) for Enhanced Dynamic Performance of High-Rise Buildings (Ph. D. thesis), 2011.
[27] B. Spencer Jr., S. Nagarajaiah, State of the art of structural control, Journal of structural engineering 129 (2003) 845–856.
[28] A. Bathaei, S.M. Zahrai, M. Ramezani, Semi-active seismic control of an 11-DOF building model with TMD + MR damper using type-1 and-2 fuzzy algorithms, J. Vib. Control 24 (2018) 2938–2953.
[29] N. Fisco, H. Adeli, Smart structures: Part II – Hybrid control systems and control strategies, Sci. Iran. 18 (2011) 285–295.
[30] T. Asai, Structural Control Strategies for Earthquake Response Reduction of Buildings (Ph.D. thesis), University of Illinois at Urbana-Champaign, 2014.
[31] S.H. Lee, D.I. Son, J. Kim, K.W. Min, Optimal design of viscoelastic dampers using eigenvalue assignment, Earthq. Eng. Struct. Dyn. 33 (2004) 521–542.
[32] C.H. Lee, Y.K. Ju, J.K. Min, S.H. Lho, S.D. Kim, Non-uniform steel strip dampers subjected to cyclic loadings, Eng. Struct. 99 (2015) 192–204.
[33] R.W. Chan, F. Albermani, Experimental study of steel slit damper for passive energy dissipation, Eng. Struct. 30 (2008) 1058–1066.
[34] ASTM D412-16, Standard Test Methods for Vulcanized Rubber and Thermoplastic Elastomers—Tension, 2016.
[35] ASTM A370-17a, Standard Test Methods and Definitions for Mechanical Testing of Steel Products, ASTM International, West Conshohocken, PA, 2017.
[36] American Society of Civil Engineers, Minimum Design Loads and Associated Criteria for Buildings and Other Structures, ASCE Reston, VA, 2017.
[37] M. Montgomery, C. Christopoulos, Experimental validation of viscoelastic coupling dampers for enhanced dynamic performance of high-rise buildings, J. Struct. Eng. 141 (2014) 04014145.
[38] S. Gong, Y. Zhou, Experimental study and numerical simulation on a new type of viscoelastic damper with strong nonlinear characteristics, Struct. Control Health Monit. 24 (2017) e1897.
[39] ABAQUS Analysis User's Manual, Version 6.13, 2014.